remote sensing

Technical Note

Directional and High-Gain Ultra-Wideband Bow-Tie Antenna for Ground-Penetrating Radar Applications

Shuai Pi [1,2], Tianhao Wang [1,2,*] and Jun Lin [1,2]

[1] College of Instrumentation and Electrical Engineering, Jilin University, Changchun 130021, China; pishuai21@mails.jlu.edu.cn (S.P.); lin_jun@jlu.edu.cn (J.L.)
[2] Key Laboratory of Geophysical Exploration Equipment, Jilin University, Ministry of Education of China, Changchun 130021, China
* Correspondence: wangtianhao@jlu.edu.cn

Abstract: Bow-tie antennas are utilized extensively in ground-penetrating radar (GPR) systems. In order to achieve sufficient penetration depth and resolution, the bow-tie antennas for GPR applications require low operating frequency, high gain, and excellent broadband. A novel ultra-wideband (UWB) bow-tie antenna with gain enhancement for GPR applications is proposed in this paper. First, a UWB bow-tie antenna with resistive loading is designed. The metal reflector and metamaterial loading make the bow-tie antenna directional, and loading the same metamaterial on the front side of the antenna further improves directional gain. After testing, the lowest frequency of the fabricated antenna is 317 MHz, the relative bandwidth is 98.6%, the peak gain in the frequency range is 9.3 dBi, and the size is only 0.38 λ at the lowest frequency. The proposed compact antenna takes both gain and bandwidth into consideration. Finally, in order to further verify the effectiveness of the proposed antenna in the GPR system, a stepped frequency continuous wave ground-penetrating radar (SFCW-GPR) system was built. The experimental results show that the designed antenna is suitable for the GPR system of deep penetration and high-resolution detection, which is beneficial to the imaging of underground structures.

Keywords: ground-penetrating radar (GPR); bow-tie antenna; high gain; metamaterial; ultra-wideband (UWB)

Citation: Pi, S.; Wang, T.; Lin, J. Directional and High-Gain Ultra-Wideband Bow-Tie Antenna for Ground-Penetrating Radar Applications. *Remote Sens.* **2023**, *15*, 3522. https://doi.org/10.3390/rs15143522

Academic Editors: David Gomez-Ortiz, Xuan Feng and Yan Su

Received: 19 June 2023
Revised: 10 July 2023
Accepted: 11 July 2023
Published: 12 July 2023

1. Introduction

Ground-penetrating radar (GPR) is a nondestructive detection instrument that analyzes subsurface constitution and identifies buried objects. It is widely used in tunnel detection, ice thickness measurement, and groundwater exploration [1–4]. Given its high speed of data acquisition and high imaging resolution, GPR has been recognized as one of the important tools for near-surface detection [5–9]. The GPR system radiates high-frequency electromagnetic waves to the ground through the antenna and receives the reflected signal due to the difference in the electrical parameters of the subsurface medium [10]. Therefore, the performance of the antenna directly determines the imaging effect of the GPR system. Ultra-wideband (UWB) technology can achieve high-resolution imaging [11], and it is relatively easy to implement UWB for antennas operating at frequencies higher than 1 GHz [12–15]. It is well known that the subsurface lossy medium causes electromagnetic waves to decay rapidly, thus the antenna should be designed to have a low operating frequency to achieve sufficient penetration depth. However, simultaneously obtaining low operating frequency, high gain, and large bandwidth has been a challenge for GPR antenna design [16].

In general, TEM horn antennas [17], Vivaldi antennas [18], and bow-tie antennas [19] are suitable for GPR systems. Among them, bow-tie antennas are widely used because of their simple structure, low profile, and linear phase characteristics in the operating frequency range [20]. A few previous studies have designed UWB bow-tie antennas. The folded bow-tie antenna designed by Serhir et al. [21] covers a bandwidth of 0.5–3 GHz, but the reflection coefficient of the antenna is higher than −10 dB at frequencies below 800 MHz, which seriously degrades the performance of the antenna in the low-frequency range. Li et al. [22] applied the Wu-King profile to improve the bandwidth of the bow-tie antenna, but the gain is less than 0 dBi in the operating frequency range of 250 MHz to 750 MHz. The loss effect of the subsurface medium becomes more serious as the depth increases. Thus, the gain of the GPR antenna is crucial for detection. However, due to the unconcentrated radiation energy of omnidirectional dipole antennas, it is extremely difficult for bow-tie antennas to achieve high gain at low operating frequencies of several hundred MHz, and the average gain of ordinary bow-tie antennas is only approximately 2–3 dBi, which cannot guarantee the effective detection depth of GPR systems [23]. Ajith et al. [24] proposed a bow-tie antenna based on loop loading and multilayer loop directors with impedance bandwidth ranging from 420 MHz to 5.5 GHz and an average gain of up to 7.2 dBi. However, the gain is less than 5 dBi at frequencies below 1 GHz.

For GPR systems, backward radiated energy in the opposite direction to the ground is useless. Traditionally, a shielding backed cavity or metal reflector is used to load the backside of a bow-tie antenna to reflect backward energy to the forward direction to improve the directional gain of the antenna. Backside loading is a significant improvement for bow-tie antennas with high operating frequencies because the height of the cavity or reflector is acceptable at short operating wavelengths [25,26]. When the bow-tie antenna operates at several hundred MHz, the height limit of $1/4\ \lambda$ makes the profile of the antenna too high. Low profile is a key characteristic required for GPR antennas [27]. If the profile is directly reduced, the impedance bandwidth will be deteriorated by the strong coupling between the backed cavity or the metal reflector and the antenna. Even though this problem can be alleviated by adding absorbing material between the cavity and the antenna, the directional gain is attenuated [28]. Metamaterials have been recently used for enhancing antenna gain [29]. Wang et al. [30] used a metamaterial lens to realize a high-gain bow-tie antenna with a bandwidth of 1.7–2.1 GHz and an average gain of more than 10 dBi, but the antenna's size is excessively large. Dan et al. [31] proposed a low-profile bow-tie antenna using an artificial magnetic conductor (AMC) reflector, and the peak gain in the frequency range of 1.19–2.37 GHz could reach 6 dBi. However, the problem is that the zero-reflection phase characteristic of AMC reflectors has difficulty taking effect at frequencies below 1 GHz and it cannot be applied to the low-frequency UWB bow-tie antenna.

Bow-tie antennas used in GPR systems have requirements in terms of bandwidth, gain, directivity, and low profile, and it is difficult for a single optimization method to consider all the characteristics. This study designs a UWB bow-tie antenna with a multilayer structure to achieve directional radiation and high gain. In Section 2, a bow-tie antenna working at low frequencies is designed based on resistive loading. Aiming at the problem of deteriorating the impedance bandwidth of the antenna when the metal reflector is loaded at a low profile, a metamaterial with periodic units is introduced between the metal reflector and the antenna to improve the radiation characteristics of the bow-tie antenna. The same metamaterial is loaded on the front side of the antenna as a directional gain enhancer, and the forward gain of the bow-tie antenna is further improved. In Section 3, the actual fabricated antenna is tested, and the performance of bow-tie antennas in other published papers is compared. In Section 4, a stepped frequency continuous wave ground-penetrating radar (SFCW-GPR) system is built by combining the vector network analyzer and the proposed antenna. The performance and practical application effect of the antenna are verified by a sand tank experiment and outdoor experiment.

2. Antenna Design and Simulation

2.1. Resistive Loaded Bow-Tie Antenna

The bow-tie antenna with a planar structure is evolved from a three-dimensional biconical antenna, and the radiating element is a pair of metal patches on a dielectric substrate. The arms of the traditional bow-tie antenna are triangular or asymmetric lozenges.

In commercial GPR systems, the triangular antenna arm is the most common, and the basic parameters include the arm length L, the field angle θ, and the distance d between the feed points, as shown in Figure 1. The operating characteristics of a bow-tie antenna can be described according to the following empirical formula:

$$Z = 120\ln(L\cot(\frac{\theta}{4})/\cos(\frac{\theta}{2})), \tag{1}$$

$$\lambda = 2L \times \sqrt{\varepsilon_{eff}}, \tag{2}$$

where Z is the characteristic impedance of the antenna, λ is the wavelength in the air, corresponding to the expected lowest operating frequency, and ε_{eff} is the effective dielectric constant of the dielectric substrate in the air.

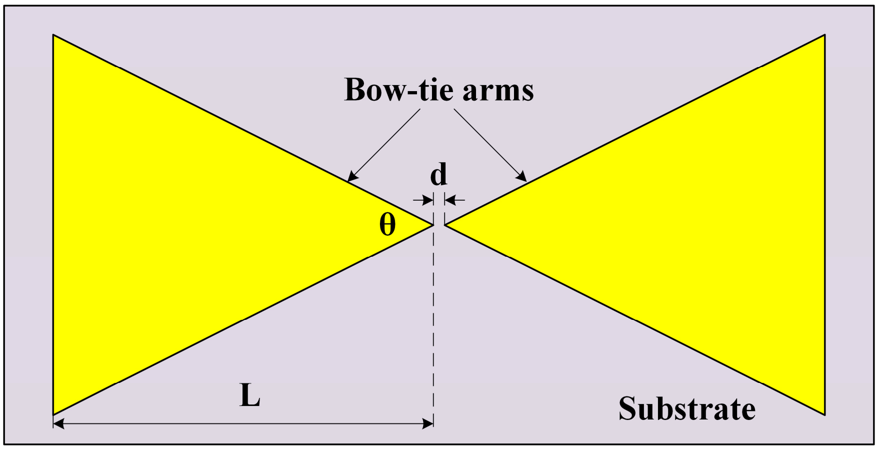

Figure 1. Traditional bow-tie antenna.

In order to connect with a general 50 Ω microwave system, the characteristic impedance of the antenna is usually designed to be close to 50 Ω. When the field angle θ of the traditional bow-tie antenna is small, the impedance is usually large, and an additional impedance converter needs to be designed [32], which complicates the structure of the antenna. Increasing the field angle θ is beneficial to reduce impedance, but the triangular arms increase the size of the antenna. The truncated arm is a common method to reduce the size of the bow-tie antenna while improving the bandwidth [33]. In this section, on the basis of the truncated arm, a bow-tie antenna is designed by adding slots, loading resistors, and fillet operation.

The proposed antenna structure is shown in Figure 2. The original shape of the antenna arm is a pentagon. Based on this, the two obtuse corners are rounded with a radius of curvature r = 20 mm. The fillet operation is conducive to improving the highest operating frequency of the antenna, which is similar to the principle of a UWB half-ellipse antenna to achieve ultra-wideband [9]. Further, a long and narrow slot is added to each arm, and the distance W_1 from the edge of the antenna arm is 40 mm. The width W_2 of the slot is designed to be 5 mm to match the chip resistor with a large size that can withstand high power, and the resistors R_1–R_4 with the same value are loaded at both ends of each slot. The resistors increase the loss of the antenna, but given that the return loss of the bow-tie antenna will deteriorate after loading the metal reflector, which may cause the S_{11} curve to be higher than −10 dB, the return loss of the single bow-tie antenna should be as good as possible in the operating frequency range. The substrate is made of FR-4 material with dielectric constant ε_r = 4.6 and thickness d_1 = 1.6 mm. The arms of the antenna are printed on both sides of the dielectric substrate, the length L_0 of the substrate is 360 mm, and the width W_0 is 250 mm. The field angle θ of the antenna is at the center of the substrate. In order to facilitate feeding, a transmission line extending to the edge of the substrate is added.

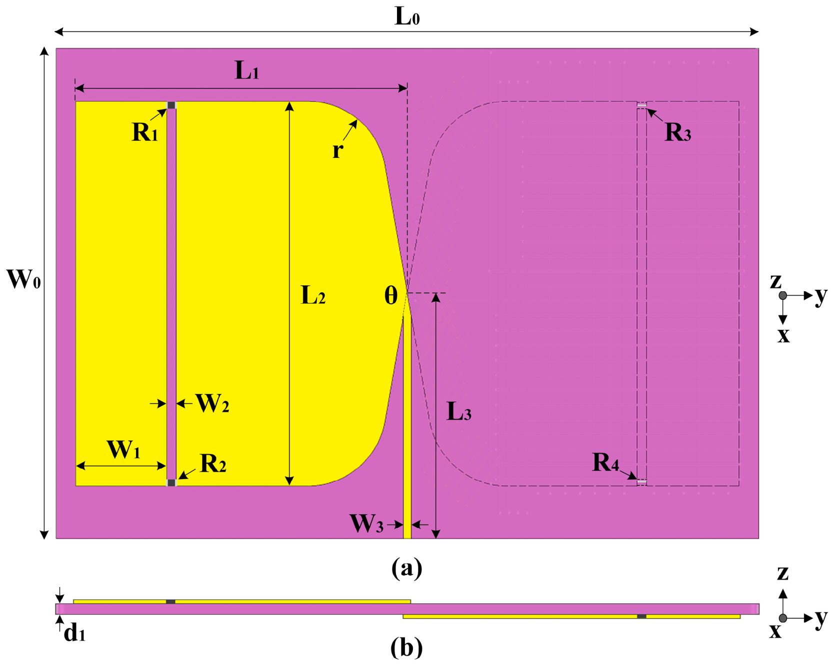

Figure 2. Structure of the resistive loaded bow-tie antenna: (**a**) The xy-plane of the antenna; (**b**) the yz-plane of the antenna.

The arm length L_1, the resistance loading position W_1, and the values of the resistances R_1–R_4 are the key parameters that affect the performance of the bow-tie antenna. We analyze the influence of these parameters on the bandwidth and gain by simulation in CST Microwave Studio. Figure 3a,b show the effect of arm length L_1. Increasing L_1 is beneficial to improve the antenna gain and can lower the lowest operating frequency of the antenna, but it will deteriorate the performance of the antenna at high frequencies and the matching in the frequency range. The arm length L_1 = 170 mm is a compromise parameter. Figure 4a,b show the effect of the resistors on the performance of the antenna. When the value of resistors R_1–R_4 is 50 Ω, the antenna's performance is better at low frequencies, but the gain in the frequency range is lower. The value of the resistor is set to 100 Ω to balance the gain and the lowest operating frequency. According to Figure 5a,b, the closer the resistors are located to the transmission line, the narrower the impedance bandwidth of the antenna and the smaller the gain. When the position of the resistor is close to the edge of the arm, the impedance bandwidth and gain of the antenna are improved, but the S_{11} curve around the center frequency is already close to −10 dB. The S_{11} curve of the single bow-tie in the frequency range should be as low as possible, so W_1 = 40 mm is appropriate for the overall design of the antenna. The final parameters of the antenna are shown in Table 1.

Figure 6 compares the surface current distribution at 500 MHz before and after optimization. The slots and the resistors improve the current distribution and direct the current to the end of the antenna arm. Meanwhile, it can be seen from Figure 7a,b that the operating frequency of the basic bow-tie antenna with pentagonal arms is not continuous. The S_{11} curve is higher than −10 dB in the range of 428 MHz to 746 MHz. Although the radiation efficiency of the bow-tie antenna is reduced in the low-frequency part after adding resistors, it is obvious that the resistive loading can improve the matching characteristics of the antenna, and the S_{11} curve in the operating frequency range is always lower than −10 dB. In addition, the highest operating frequency of the antenna is improved due to the fillet operation. In the simulation, the antenna impedance bandwidth is 339–970 MHz, which allows GPR to achieve high-resolution imaging. The radiation pattern of a single bow-tie antenna at frequencies from 400 MHz to 900 MHz is shown in Figure 8. The antenna has a clear main lobe in the +z and –z directions. Given that the energy radiation is not directional, the gain is only 2 dBi to 3 dBi. In GPR applications, the backward radiation in the opposite direction to the ground is deemed to be useless and, thus, focusing the energy forward is necessary in order to enhance the directional gain.

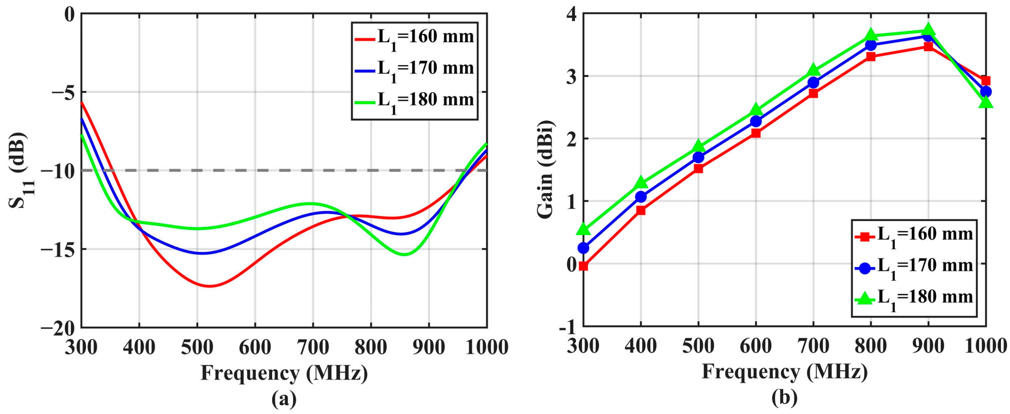

Figure 3. Simulation results for different values of L_1: (**a**) Return loss; (**b**) gain. (W_1 = 40 mm, R_1–R_4 = 100 Ω).

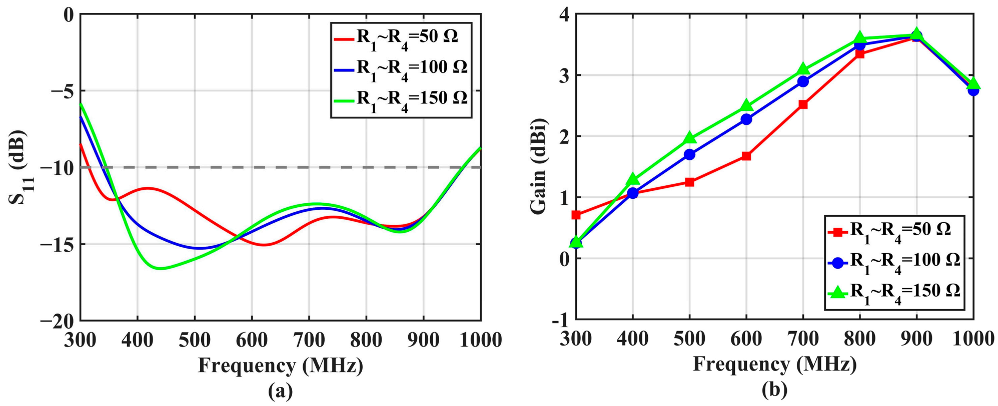

Figure 4. Simulation results for different values of R_1–R_4: (**a**) Return loss; (**b**) gain. (L_1 = 170 mm, W_1 = 40 mm).

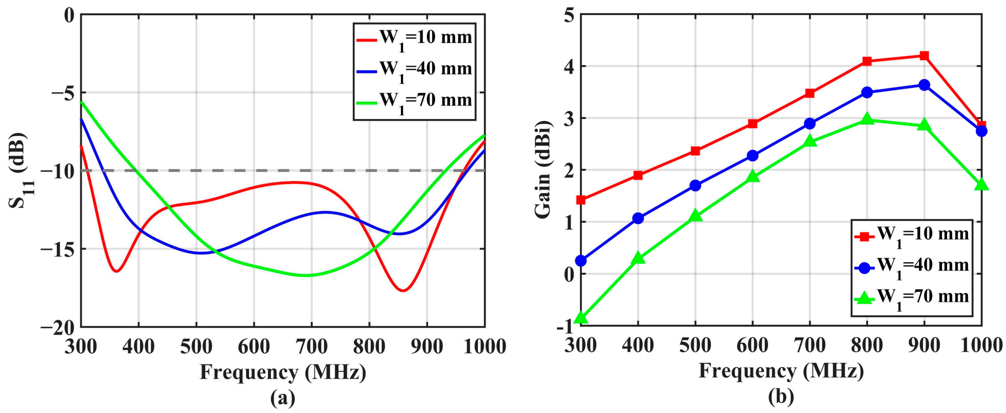

Figure 5. Simulation results for different values of W_1: (**a**) Return loss; (**b**) gain. (L_1 = 170 mm, R_1–R_4 = 100 Ω).

Table 1. Parameters of the bow-tie antenna.

Parameter	W_0	W_1	W_2	W_3	r	L_0	L_1	L_2	L_3	θ
Value	250 mm	40 mm	5 mm	3.8 mm	20 mm	360 mm	170 mm	196 mm	125 mm	160°

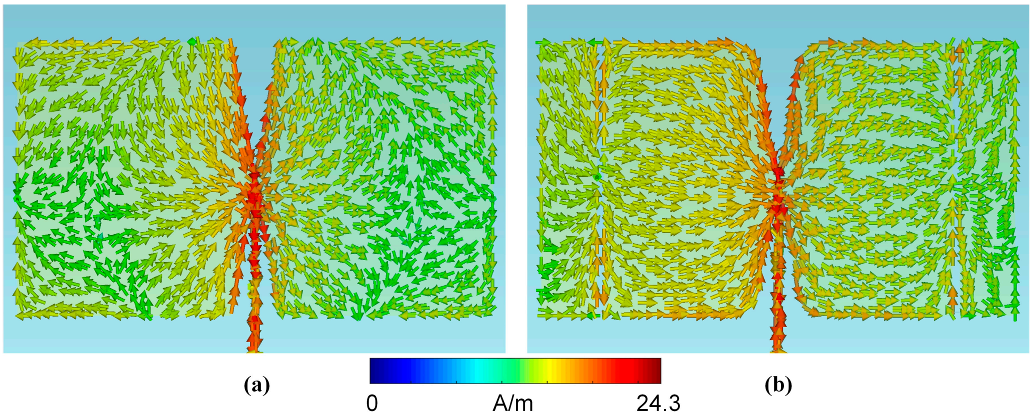

Figure 6. Surface current distributions: (**a**) Basic bow-tie antenna; (**b**) proposed bow-tie antenna.

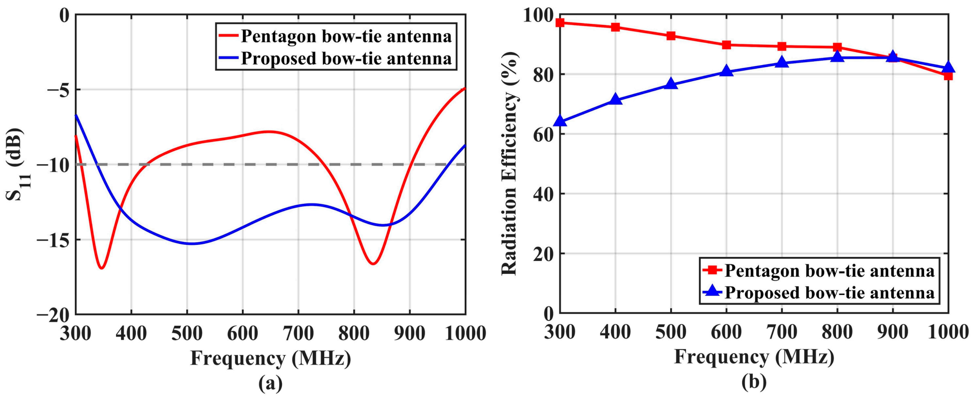

Figure 7. Comparison of bow-tie antennas: (**a**) Return loss; (**b**) radiation efficiency.

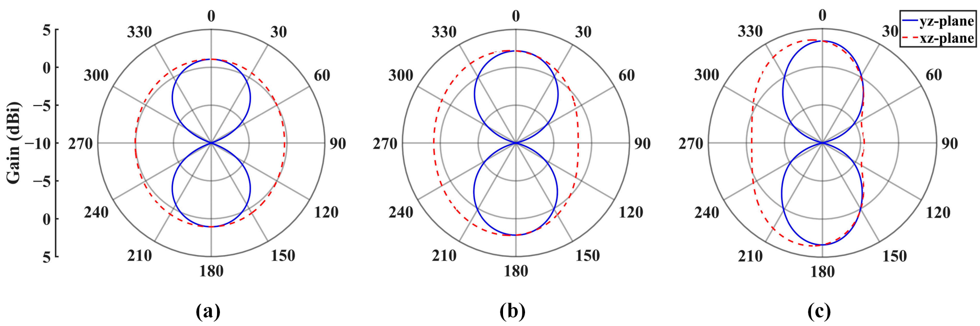

Figure 8. Radiation pattern of a single bow-tie antenna: (**a**) 400 MHz; (**b**) 600 MHz; (**c**) 900 MHz.

2.2. Metal Reflector and Metamaterial

Initially, we tentatively loaded a metal reflector in order to enhance the forward gain. Metal reflectors mainly rely on the metal surface to reflect electromagnetic waves, and the thickness of the metal has no effect on the reflection characteristics, which can be achieved by printing a complete metal surface onto an inexpensive FR-4 substrate. As shown in Figure 9, the metal reflector is loaded on the backside of the bow-tie antenna at height h_1. The thickness d_2 is 1.6 mm, the dielectric constant ε_r is 4.6, and the side of the printed metal surface faces the bow-tie antenna. The substrate is a square of 360 mm × 360 mm, and the side length is the same as the length L_0 of the bow-tie antenna. Figure 10a,b show the simulation results of the return loss of the antenna and the gain in the $-z$ direction at different h_1. The metal reflector can enhance the directional gain, but the S_{11} curve in part of the frequency range is higher than -10 dB, and the impedance bandwidth is deteriorated. Increasing the height h_1 of the reflector will alleviate the return loss, however, the gain will be seriously reduced and the profile is excessively high, which is unfavorable for GPR systems.

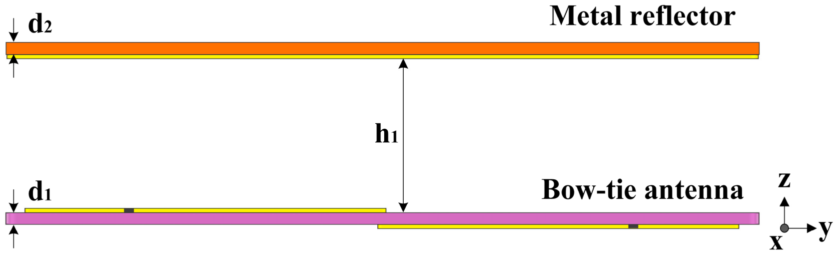

Figure 9. Structure of bow-tie antenna with a metal reflector.

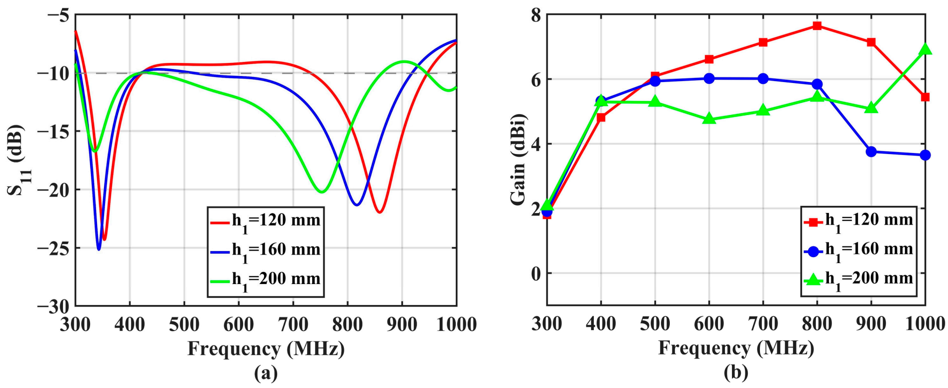

Figure 10. Simulation results for different values of h_1: (**a**) Return loss; (**b**) gain.

This study designs a metamaterial with artificial periodic units to improve the radiation characteristics of a low-profile bow-tie antenna loaded with a metal reflector. Figure 11 shows the structure of the bow-tie antenna with a metamaterial and a metal reflector, and the height h_1 of the metal reflector is set to 120 mm. The metamaterial is located between the metal reflector and the bow-tie antenna, and the height h_2 from the bow-tie antenna is 10 mm. Different from the zero-reflection phase characteristic of the AMC reflector, the proposed metamaterial is located closer to the antenna. The close loading of metamaterial can enhance the coupling between the metamaterial and the antenna and improve the impedance of the antenna when loading a metal reflector. The metamaterial is printed on one side of the FR-4 dielectric substrate. The thickness d_3 is 1.6 mm, the dielectric constant ε_r is 4.6, and the shape remains the same as the metal reflector. To match the dimensions, we design the metamaterial as a 6×6 array, and the side length D_1 of the periodic unit is 60 mm. The period unit of the metamaterial is a metal ring with a width D_3 of 10 mm, as shown in Figure 12a. The antenna relies on the metal reflector to reflect electromagnetic waves, meaning that the metamaterial possesses advantageous transmission properties. We simulate the metamaterial unit under periodic boundary conditions. Figure 12 shows the effect of the outer diameter D_2 of the ring on the metamaterial. The larger the outer diameter D_2 of the ring, the worse the transmission coefficient of the metamaterial, and the lower the gain of the antenna in the -z direction. However, at the same time, the matching degree in the operating frequency range becomes better with the increase in D_2. By comparison, it is found that the antenna has the widest impedance bandwidth when D_2 = 53 mm, and the gain in the low-frequency part is considered.

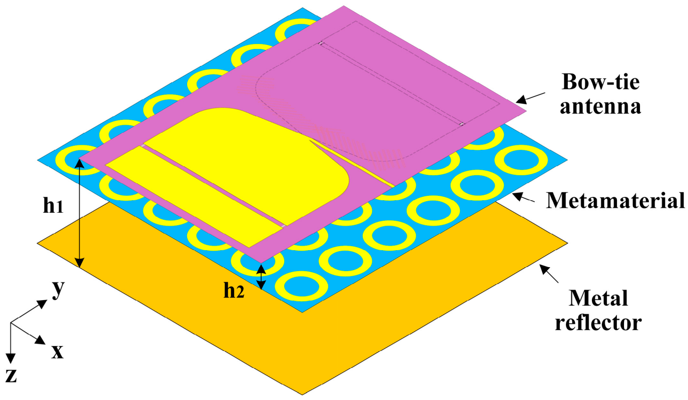

Figure 11. Structure of bow-tie antenna with a metamaterial and a metal reflector.

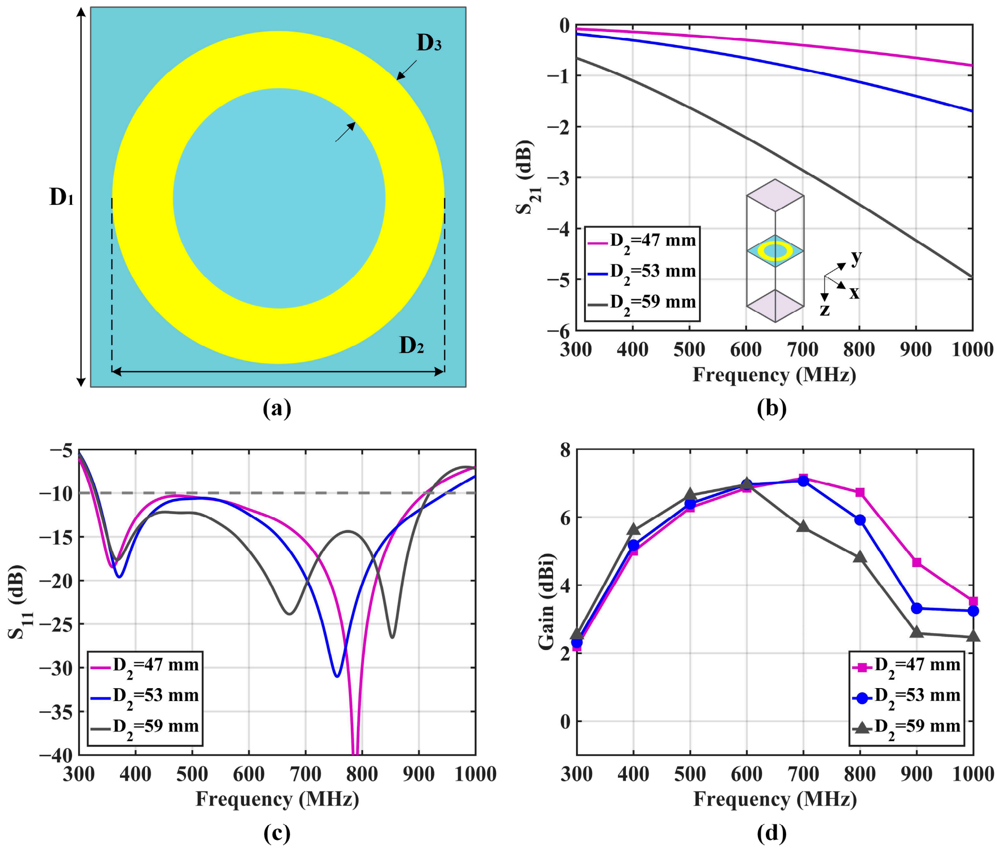

Figure 12. (**a**) Metamaterial unit; (**b**) transmission coefficient at different D_2; (**c**) return loss of the antenna at different D_2; (**d**) gain of the antenna in the −z direction at different D_2.

Figure 13a compares the return loss of the single bow-tie antenna, the antenna with a metal reflector, and the antenna with a metamaterial and a metal reflector in simulation. Without increasing the antenna profile, loading metamaterial can alleviate the deterioration of S_{11} by the metal reflector. In the frequency range of 331 MHz to 921 MHz, the S_{11} curve is less than −10 dB, which reflects that the metamaterial is effective in improving the radiation characteristics of the antenna. Figure 13b shows that, compared with the original bow-tie antenna, the gain of the antenna with a metamaterial and a metal reflector in the −z direction is significantly enhanced, and the peak gain reaches 7 dBi. The radiation patterns of the antenna at 400 MHz, 600 MHz, and 900 MHz are shown in Figure 14. Compared with Figure 8, the antenna has directivity, the main lobe in the −z direction is clear, and no side lobes are found.

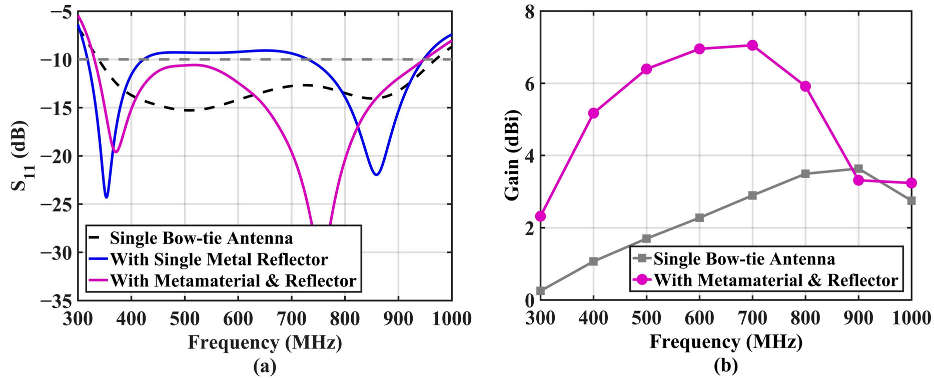

Figure 13. Comparison of different antenna structures: (**a**) Return loss; (**b**) gain in the −z direction.

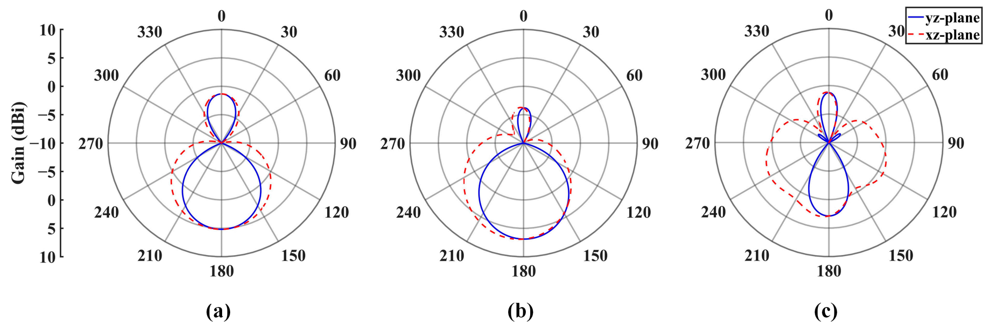

Figure 14. Radiation pattern of the antenna with a metamaterial and a metal reflector: (**a**) 400 MHz; (**b**) 600 MHz; (**c**) 900 MHz.

2.3. Directional Gain Enhancer

In the simulation, we found that loading the proposed metamaterial on the front side of the bow-tie antenna can further enhance the directional radiation performance. For antenna fabrication, using the same metamaterial is a low-cost implementation method. Thus, the metamaterial is loaded in the forward direction of the bow-tie antenna as a directional gain enhancer. Figure 15 shows the overall structure of the antenna system. The two metamaterials are shown in different colors to make the figure more intuitive. We analyze the effect of h_3 on the impedance bandwidth and the gain in the −z direction of the antenna, as shown in Figure 16a,b. Increasing h_3 is beneficial to enhance the directional gain below 700 MHz, but the impedance bandwidth is reduced. Considering the height of the antenna profile, h_3 = 80 mm is an appropriate value. Figure 17 compares the gain in the −z direction of different antenna structures, and the peak gain of the bow-tie antenna after loading the directional gain enhancer is 9.2 dBi. Compared with the antenna with metamaterial and metal reflector, the gain at 800 MHz is enhanced by 3.2 dB and shows a significant gain enhancement effect in the operating frequency range, which can make the depth exploration ability of the GPR system stronger.

The GPR system requires the antenna to have good waveform fidelity. We further simulated the time-domain characteristics of the antenna in free space. The input signal is a Gaussian pulse, and the electric field probe is placed at a distance of 1 m from the antenna in the −z direction. Figure 18 shows that the waveform of the pulse radiated by the antenna is good, without obvious distortion, and has a low ringing amplitude, which proves that the antenna can meet the requirements of the GPR system.

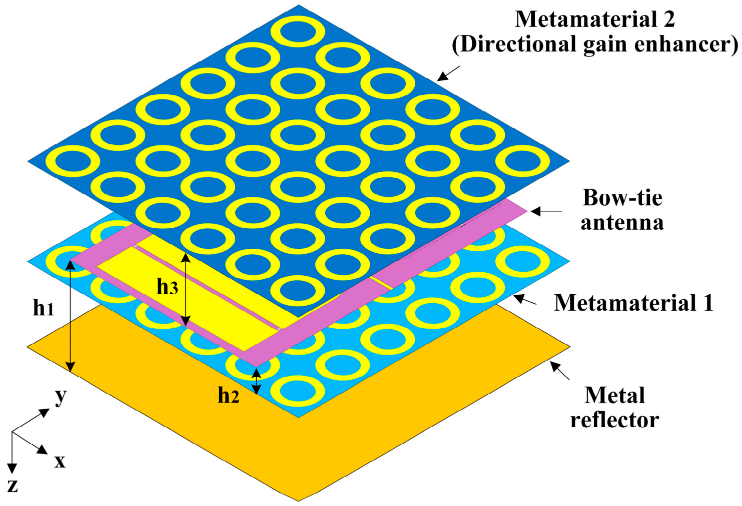

Figure 15. Overall structure of the antenna system.

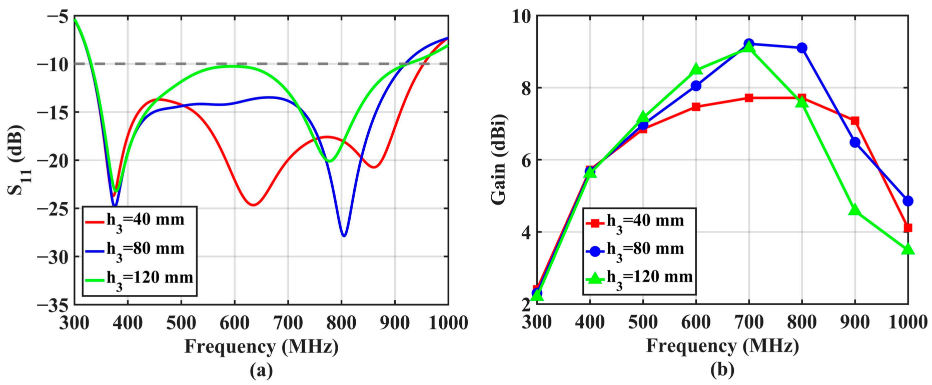

Figure 16. Simulation results for different values of h_3. (**a**) Return loss; (**b**) gain in the −z direction.

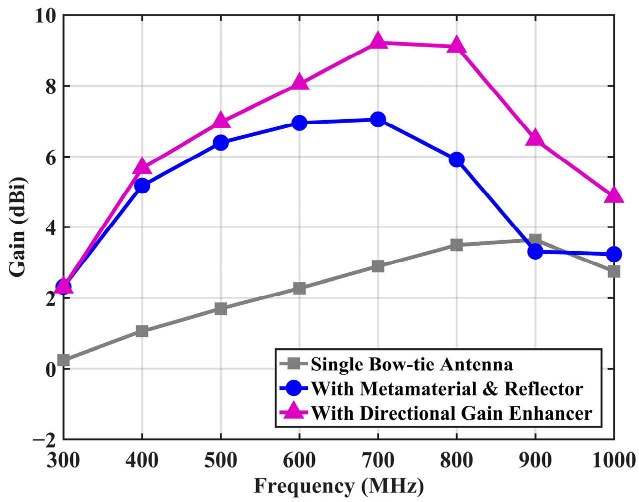

Figure 17. Simulation results of the gain in the −z direction for different antenna structures.

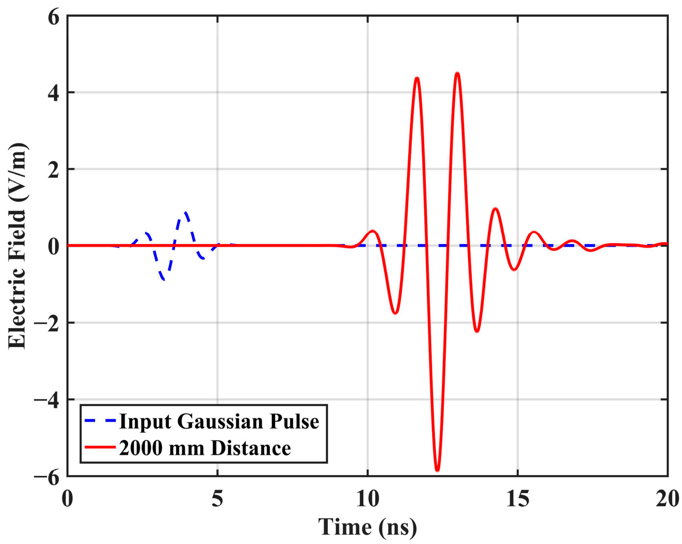

Figure 18. Simulation results of the time-domain response of the antenna system.

3. Results and Discussion

The fabricated bow-tie antenna, metal reflector, metamaterial, and the overall antenna system are shown in Figure 19. The parts of the antenna system are connected by mounting holes, nylon struts, and nylon nuts. The 50 Ω chip resistors used on the bow-tie antenna are MCR100JZHF1000 produced by ROHM Semiconductor. The parametric test of the antenna is carried out in a microwave anechoic chamber, and the measurement scenario is shown in Figure 20a. The comparisons between the measured and simulated results are shown in Figure 20b,c. The measured operating frequency range of the antenna is 317–934 MHz, the relative bandwidth is 98.6%, and the matching within the operating frequency range is good. Compared with the simulation results of return loss, the impedance bandwidth of the actually fabricated antenna is slightly wider. The measured gain of the antenna in the −z direction is consistent with the simulated results, and the peak gain is 9.3 dBi. Figure 21 shows the measured radiation patterns of the antenna in the xz-plane and yz-plane at 400 MHz, 700 MHz, and 900 MHz, respectively. The measured results show that the antenna has strong directivity and a clear main lobe, which meets the requirements of the directional radiation of GPR systems.

Table 2 compares bow-tie antenna designs in other published papers and demonstrates the strengths of this work. In [11], a UWB bow-tie antenna with low dispersion is designed with a peak gain of 3.7 dBi in the operating bandwidth (250 MHz to 780 MHz). In Ref. [22], the antenna bandwidth is extended by loading 64 resistors on the half-elliptical-shaped arms, but the peak gain within the operating bandwidth (250 MHz to 750 MHz) is only −7.5 dBi. In this case, the transmitter of GPR needs to be configured with extremely high power; otherwise, the penetration of electromagnetic waves into the subsurface lossy medium cannot be guaranteed. The authors of [24] designed a bow-tie antenna with parasitic loops with impedance bandwidth covering from 420 MHz to 5.5 GHz, but the gain below 900 MHz is less than 5 dBi and nondirectional. The authors of [29] designed a directional high-gain bow-tie antenna using an inductive reflector, but it cannot be used in the GPR system for deep underground target detection because the lowest frequency is 800 MHz. The authors of [34] designed a folded bow-tie antenna based on a combination of capacitive and resistive loading, which has a minimum operating frequency of 250 MHz but a peak gain of only 4 dBi. In this work, the lowest operating frequency of the antenna is 317 MHz, the relative bandwidth is 98.6%, the peak gain is 9.3 dBi, and the size of the antenna is only 0.38 $\lambda_l \times 0.38\ \lambda_l$ (λ_l is the wavelength corresponding to the lowest operating frequency). Based on the above analysis, it can be found that the bow-tie antenna proposed in this paper achieves low operating frequency, high gain, and large bandwidth simultaneously, which has obvious advantages over other antennas mentioned in Table 2 in GPR applications.

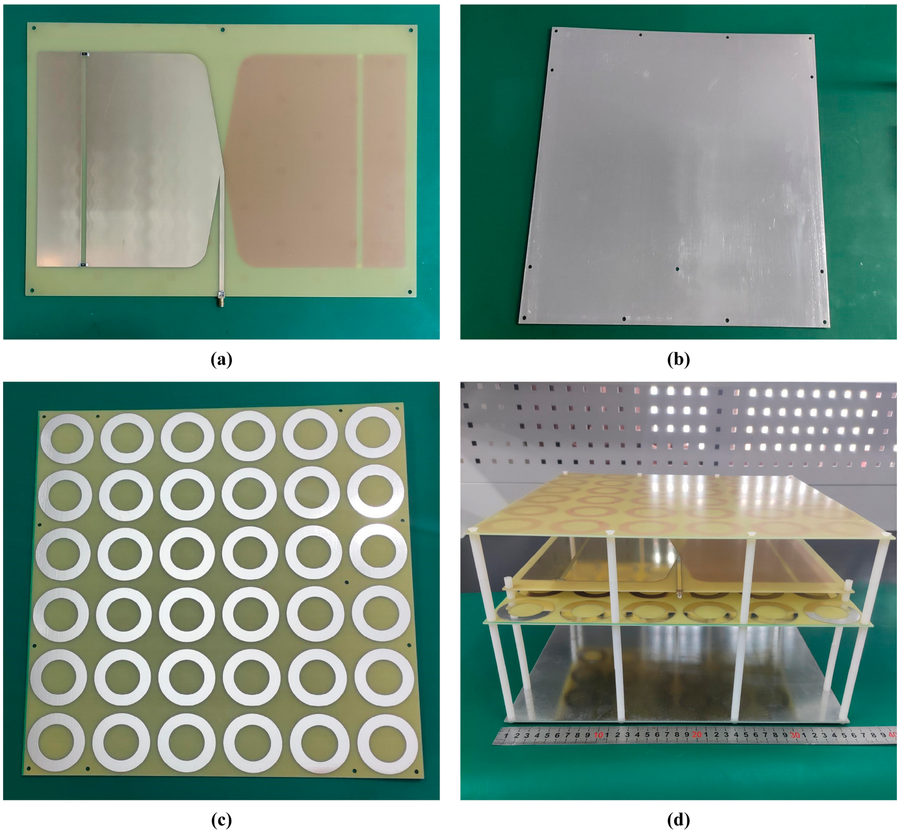

Figure 19. Fabricated antenna: (**a**) Bow-tie antenna; (**b**) metal reflector; (**c**) metamaterial; (**d**) antenna system.

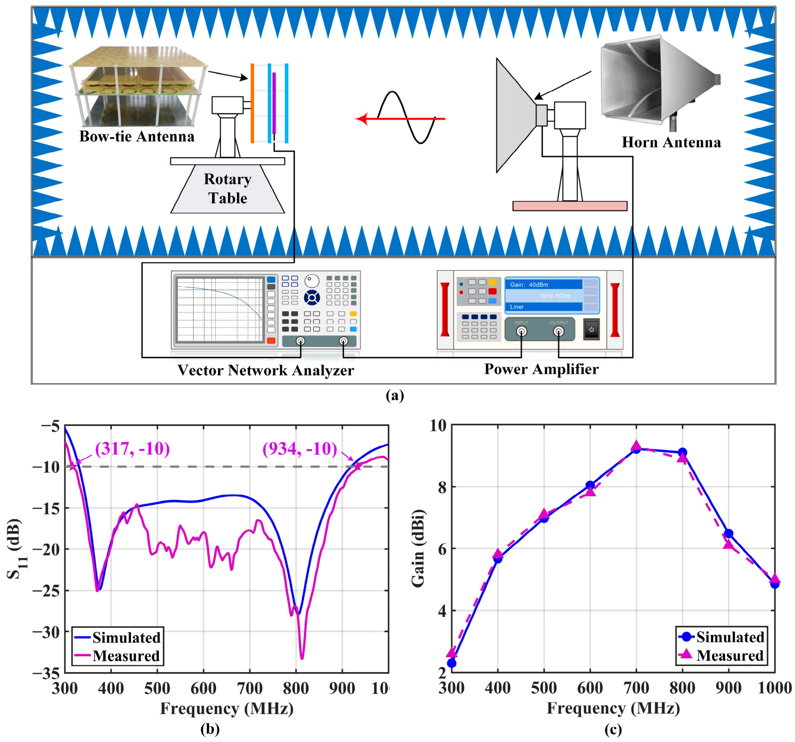

Figure 20. The measurement scenario and the comparison of measured and simulated results: (**a**) The measurement scenario; (**b**) return loss; (**c**) gain in the -z direction.

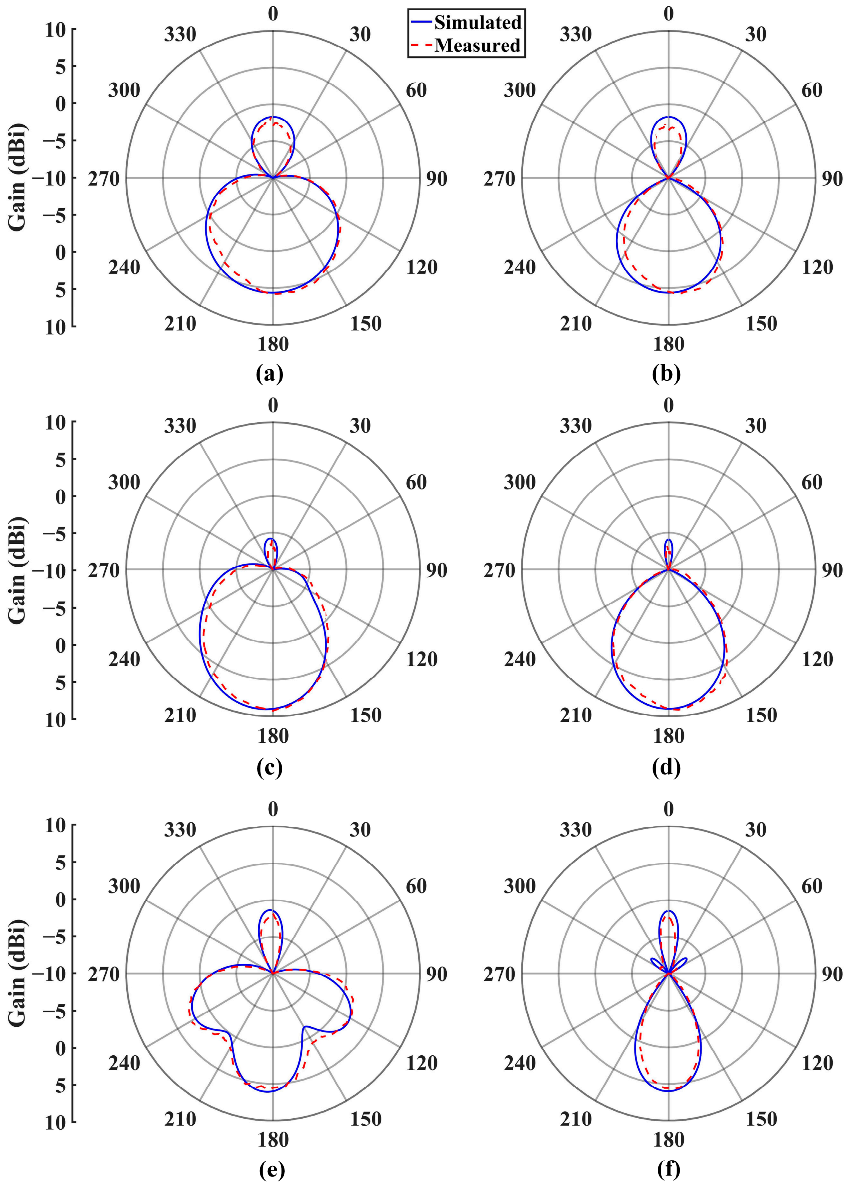

Figure 21. Comparison of measured and simulated radiation patterns at different frequencies: (**a**) xz-plane at 400 MHz; (**b**) yz-plane at 400 MHz; (**c**) xz-plane at 700 MHz; (**d**) yz-plane at 700 MHz; (**e**) xz-plane at 900 MHz; (**f**) yz-plane at 900 MHz.

Table 2. Comparison with Other Bow-tie Antennas.

Ref.	Lowest Frequency	Bandwidth	Size	Peak Gain below 900 MHz	Application
[11]	250 MHz	102.9%	$0.38\ \lambda_l \times 0.05\ \lambda_l$	3.7 dBi	GPR
[22]	250 MHz	100%	$0.63\ \lambda_l \times 0.25\ \lambda_l$	−7.5 dBi	GPR
[24]	420 MHz	171.6%	$0.32\ \lambda_l \times 0.32\ \lambda_l$	5 dBi	GPR
[29]	800 MHz	37%	$0.60\ \lambda_l \times 0.60\ \lambda_l$	9 dBi	/
[34]	250 MHz	109%	$0.25\ \lambda_l \times 0.15\ \lambda_l$	4 dBi	GPR
This work	317 MHz	98.6%	$0.38\ \lambda_l \times 0.38\ \lambda_l$	9.3 dBi	GPR

4. Experimental Case

To verify the practical application effect of this antenna in GPR systems, we constructed an SFCW-GPR using two fabricated bow-tie antennas and a two-port vector network analyzer (Keysight N9925A) system, as shown in Figure 22. Port 1 of the vector network analyzer is used as the excitation port, Port 2 is used as the receiving port, and the two antennas are connected to the two ports through 50 Ω coaxial cables. The transmitting and receiving antennas are configured to be placed in parallel with a fixed relative distance of 6 cm. Furthermore, we used the constructed SFCW-GPR system to conduct sand tank experiments and outdoor experiments.

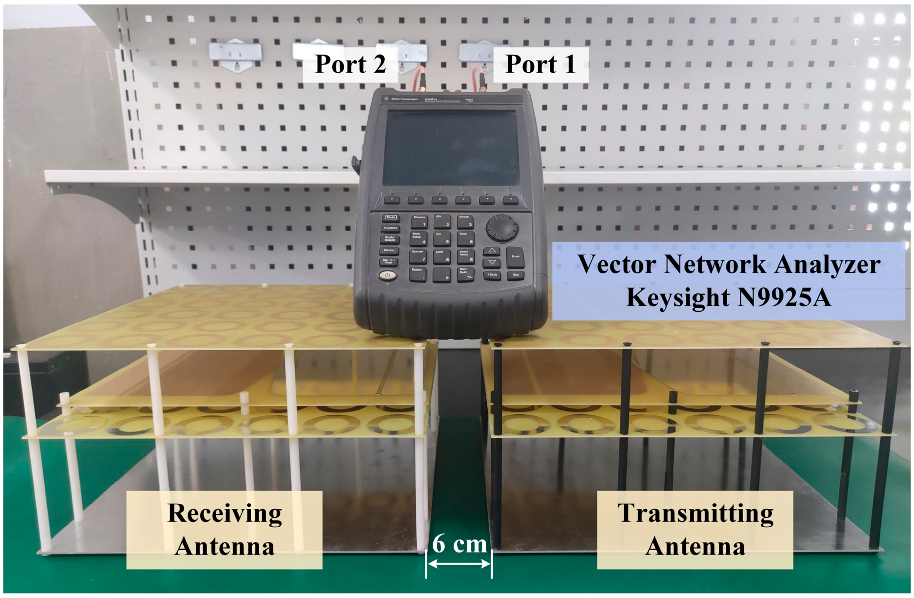

Figure 22. SFCW-GPR system based on the vector network analyzer.

4.1. Case 1: Sand Tank Experiment

First, a sand tank with buried objects was constructed in the laboratory to simulate a real outdoor subsurface structure. Figure 23a shows the structure of the sand tank. Sand is used as a lossy medium to simulate the real geological environment. The depth of the sand tank is 0.8 m, and the bottom of the tank is a concrete structure. In the sand tank, five targets are tested, including three copper pipes (Target 2,3,5) and two hollow PVC pipes (Target 1,4). The diameters and depths of the five targets from the upper surface of the sand tank are shown in Table 3. In the experiment, the total length of the survey line is 3 m, and the step movement of the SFCW-GPR system is 5 cm. The profile image along the survey line of the sand tank is shown in Figure 23b. The positions of the five targets in the sand trough can be clearly distinguished, which is consistent with the structure of the constructed sand tank, and the foundation below the sand tank can be found, which verifies that the designed antenna can be effectively applied to the GPR system.

Table 3. Attributes of Targets in Sand Tank.

Target	Material	Diameter (m)	Depth (m)
1	PVC	0.4	0.4
2	Copper	0.4	0.5
3	Copper	0.4	0.4
4	PVC	0.3	0.3
5	Copper	0.4	0.4

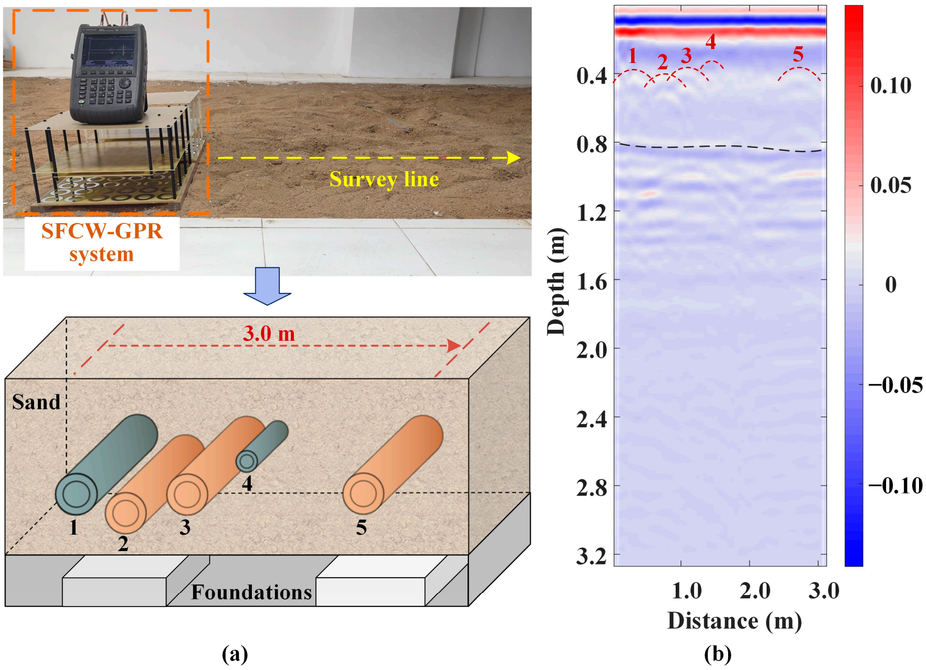

Figure 23. Sand tank experiment: (**a**) Structure of the sand tank; (**b**) profile image of the survey line.

4.2. Case 2: Outdoor Experiment

To evaluate the detection depth and imaging resolution of the constructed SFCW-GPR system, we conducted an outdoor experiment on a pedestrian road in a city. The experimental environment is shown in Figure 24a. In the experiment, the length of the survey line is approximately 30 m, and some trees with a height of more than 10 m are arranged along the survey line next to the detection area. Furthermore, there is a drainage well at the end of the survey line. Figure 24b shows the profile image of the survey line. We have performed background removal and gain processing on the original data. At 25 m, from the start of the survey line, strong reflections caused by the drainage well can be seen. From 20 ns to 40 ns in the profile image of the survey line, there are reflected waves caused by tree roots, which can be clearly distinguished. The experimental results verify that the SFCW-GPR system can achieve deep penetration detection with high resolution, which benefits from the high-gain and ultra-wideband characteristics of the proposed antenna.

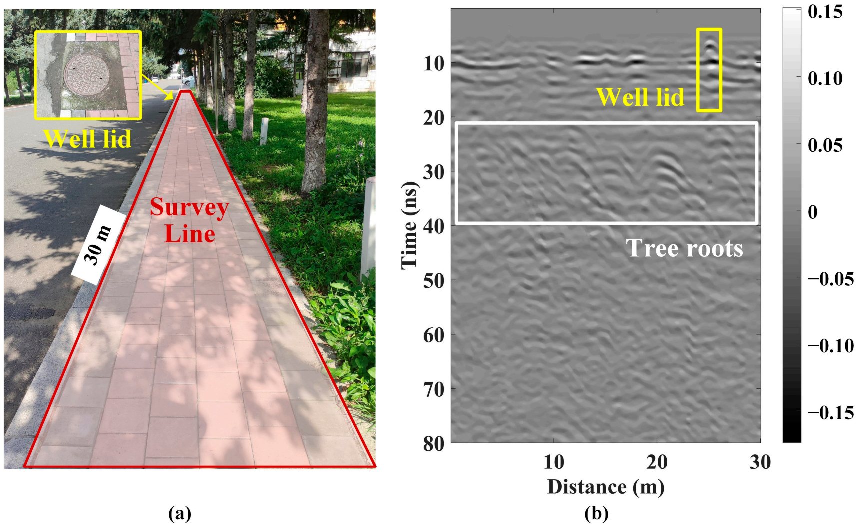

Figure 24. Outdoor experiment: (**a**) Experimental environment; (**b**) profile image of the survey line.

5. Conclusions

Antennas are the key to the GPR system to realize subsurface detection. This study proposes a directional high-gain antenna with a multilayer structure for GPR applications of deep penetration and high-resolution imaging. The UWB bow-tie antenna is designed by loading slots and resistors on the antenna arms, and the metal reflector and metamaterials are used to improve the radiation characteristics of the antenna. The operating frequency range of the fabricated antenna is 317–934 MHz, the relative bandwidth is 98.6%, the peak gain is 9.3 dBi, and the size of the antenna is only 0.38 $\lambda_l \times 0.38\ \lambda_l$. Compared with published papers, the antenna proposed in this work is compact while considering gain and bandwidth. The results of the experimental case using the constructed SFCW-GPR system show that the antenna can provide a solution for improving the performance of the GPR system.

Author Contributions: Conceptualization, S.P. and J.L.; methodology, S.P.; software, S.P.; validation, S.P., T.W. and J.L.; formal analysis, S.P. and T.W.; investigation, S.P., T.W. and J.L.; resources, T.W. and J.L.; data curation, S.P.; writing—original draft preparation, S.P. and T.W.; writing—review and editing, S.P., T.W. and J.L.; visualization, S.P.; supervision, T.W.; project administration, J.L.; funding acquisition, T.W. and J.L. All authors have read and agreed to the published version of the manuscript.

Funding: This research was supported by the Graduate Innovation Fund of Jilin University (grant number 2022053), the Key Laboratory for Comprehensive Energy Saving of Cold Regions Architecture of Education, Jilin Jianzhu University (grant number JLJZHDKF202203), and the National Natural Science Foundation of China (grant number 41827803).

Data Availability Statement: Not applicable.

Conflicts of Interest: The authors declare no conflict of interest.

References

1. Daniels, D.J. *Ground Penetrating Radar*; The Institution of Electrical Engineers: London, UK, 2004; p. 726.
2. Jol, H.M. *Ground Penetrating Radar: Theory and Applications*; Elsevier Science: Amsterdam, The Netherlands, 2009; p. 544.
3. Reynolds, J.M. *An Introduction to Applied and Environmental Geophysics*, 2nd ed.; Wiley: New York, NY, USA, 2011.
4. Wai-Lok Lai, W.; Dérobert, X.; Annan, P. A Review of Ground Penetrating Radar Application in Civil Engineering: A 30-Year Journey from Locating and Testing to Imaging and Diagnosis. *NDT E Int.* **2018**, *96*, 58–78. [CrossRef]
5. Solla, M.; Pérez-Gracia, V.; Fontul, S. A review of GPR application on transport infrastructures: Troubleshooting and best practices. *Remote Sens.* **2021**, *13*, 672. [CrossRef]
6. Srivastav, A.; Nguyen, P.; McConnell, M.; Loparo, K.A.; Mandal, S. A highly digital multiantenna ground-penetrating radar (GPR) system. *IEEE Trans. Instrum. Meas.* **2020**, *69*, 7422–7436. [CrossRef]
7. Zhou, X.; Chen, H.; Li, J. An automatic GPR B-scan image interpreting model. *IEEE Trans. Geosci. Remote Sens.* **2018**, *56*, 3398–3412. [CrossRef]
8. Zeng, Z.; Li, J.; Huang, L.; Feng, X.; Liu, F. Improving target detection accuracy based on multipolarization MIMO GPR. *IEEE Trans. Geosci. Remote Sens.* **2014**, *53*, 15–24. [CrossRef]
9. Wu, B.; Ji, Y.; Fang, G. Analysis of GPR UWB half-ellipse antennas with different heights of backed cavity above ground. *IEEE Antennas Wirel. Propag. Lett.* **2010**, *9*, 130–133. [CrossRef]
10. Aboudourib, A.; Serhir, M.; Lesselier, D. A processing framework for tree-root reconstruction using ground-penetrating radar under heterogeneous soil conditions. *IEEE Trans. Geosci. Remote Sens.* **2020**, *59*, 208–219. [CrossRef]
11. Wu, Y.; Shen, F.; Xu, D.; Liu, R. An ultra-wideband antenna with low dispersion for ground penetrating radar system. *IEEE Sensors J.* **2021**, *21*, 15171–15179. [CrossRef]
12. Ruengwaree, A.; Ghose, A.; Kompa, G. A novel UWB rugby-ball antenna for near-range microwave radar system. *IEEE Trans. Microwave Theory Tech.* **2006**, *54*, 2774–2779. [CrossRef]
13. Saitou, A.; Aoki, K.; Honjo, K.; Watanabe, K. Design considerations on the minimum size of broadband antennas for UWB applications. *IEEE Trans. Microwave Theory Tech.* **2008**, *56*, 15–21. [CrossRef]
14. Marchais, C.; Le Ray, G.; Sharaiha, A. Stripline slot antenna for UWB communications. *IEEE Antennas Wirel. Propag. Lett.* **2006**, *5*, 319–322. [CrossRef]
15. Osaretin, I.A.; Torres, A.; Chen, C.C. A novel compact dual-linear polarized UWB antenna for VHF/UHF applications. *IEEE Antennas Wirel. Propag. Lett.* **2009**, *8*, 145–148. [CrossRef]
16. Sagnard, F.; Tebchrany, E. Using polarization diversity in the detection of small discontinuities by an ultra-wide band ground-penetrating radar. *Measurement* **2015**, *61*, 129–141. [CrossRef]

17. Shao, J.; Fang, G.; Fan, J.; Ji, Y.; Yin, H. TEM horn antenna loaded with absorbing material for GPR applications. *IEEE Antennas Wirel. Propag. Lett.* **2014**, *13*, 523–527. [CrossRef]
18. Hu, Z.; Zeng, Z.; Wang, K.; Feng, W.; Zhang, J.; Lu, Q.; Kang, X. Design and Analysis of a UWB MIMO Radar System with Miniaturized Vivaldi Antenna for Through-Wall Imaging. *Remote Sens.* **2019**, *11*, 1867. [CrossRef]
19. Li, G.; Mi, J.; He, Y.; Wang, T. Design of ultra-wideband folded antenna for ground penetrating radar. In Proceedings of the 2020 IEEE 1st China International Youth Conference on Electrical Engineering (CIYCEE), Wuhan, China, 1–4 November 2020.
20. Nayak, R.; Maiti, S. A review of Bow-Tie antennas for GPR applications. *IETE Tech. Rev.* **2019**, *36*, 382–397. [CrossRef]
21. Serhir, M.; Lesselier, D. Wideband reflector-backed folded bowtie antenna for ground penetrating radar. *IEEE Trans. Antennas Propag.* **2017**, *66*, 1056–1063. [CrossRef]
22. Li, X.; Ji, Y.C.; Lu, W.; Fang, G. Analysis of GPR Antenna System Mounted on a Vehicle. *IEEE Antennas Wirel. Propag. Lett.* **2013**, *12*, 575–578. [CrossRef]
23. Li, Y.; Chen, J. Design of miniaturized high gain bow-tie antenna. *IEEE Trans. Antennas Propag.* **2021**, *70*, 738–743. [CrossRef]
24. Ajith, K.K.; Bhattacharya, A. A Novel Compact Super wide band Bowtie Antenna for 420 MHz to 5.5 GHz Operation. *IEEE Trans. Antennas. Propag.* **2018**, *66*, 3830–3836. [CrossRef]
25. Qu, S.W.; Li, J.L.; Xue, Q.; Chan, C.H. Wideband cavity-backed bowtie antenna with pattern improvement. *IEEE Trans. Antennas Propag.* **2008**, *56*, 3850–3854. [CrossRef]
26. Qu, S.W.; Li, J.L.; Xue, Q.; Chan, C.H.; Li, S. Wideband and unidirectional cavity-backed folded triangular bowtie antenna. *IEEE Trans. Antennas Propag.* **2009**, *57*, 1259–1263. [CrossRef]
27. Yektakhah, B.; Chiu, J.; Alsallum, F.; Sarabandi, K. Low-Profile, Low-Frequency, UWB Antenna for Imaging of Deeply Buried Targets. *IEEE Geosci. Remote Sens. Lett.* **2020**, *17*, 1168–1172. [CrossRef]
28. Caratelli, D.; Yarovoy, A.; Ligthart, L.P. Full-wave analysis of cavity-backed resistively loaded bow-tie antennas for GPR applications. In Proceedings of the 2008 European Radar Conference, Amsterdam, The Netherlands, 30–31 October 2008.
29. Darvazehban, A.; Rezaeieh, S.A.; Abbosh, A. Wideband beam-switched bow-tie antenna with inductive reflector. *IEEE Antennas Wirel. Propag. Lett.* **2020**, *19*, 1724–1728. [CrossRef]
30. Wang, Z.; Yang, Z.; Zeng, W.; Zhao, X.; Guo, L.; Guo, M. A high-gain bow-tie antenna with phase gradient metasurface lens. *Int. J. RF Microw. Comput.-Aided Eng.* **2021**, *31*, 22847. [CrossRef]
31. Feng, D.; Zhai, H.; Xi, L.; Yang, S.; Zhang, K.; Yang, D. A broadband low-profile circular-polarized antenna on an AMC reflector. *IEEE Antennas Wirel. Propag. Lett.* **2017**, *16*, 2840–2843. [CrossRef]
32. Van Verre, W.; Podd, F.J.; Gao, X.; Daniels, D.J.; Peyton, A.J. A review of passive and active ultra-wideband baluns for use in ground penetrating radar. *Remote Sens.* **2021**, *13*, 1899. [CrossRef]
33. Li, K.; Dong, T.; Xia, Z. Improvement of bow-tie antenna for ground penetrating radar. In Proceedings of the 2019 International Conference on Microwave and Millimeter Wave Technology (ICMMT), Guangzhou, China, 19–22 May 2019.
34. Yang, G.; Ye, S.; Ji, Y.; Zhang, X.; Fang, G. Radiation Enhancement of an Ultrawideband Unidirectional Folded Bowtie Antenna for GPR Applications. *IEEE Access* **2020**, *8*, 182218–182228. [CrossRef]